Instability in pressure-driven displacement flow of one fluid by another in a pipe

Kunal Dilip Bhagat

A Thesis Submitted to
Indian Institute of Technology Hyderabad
In Partial Fulfillment of the Requirements for
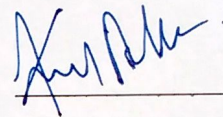The Degree of Master of Technology

भारतीय प्रौद्योगिकी संस्थान हैदराबाद
Indian Institute of Technology Hyderabad

Department of Chemical Engineering

June 2016

Declaration

I declare that this written submission represents my ideas in my own words, and where ideas or words of others have been included, I have adequately cited and referenced the original sources. I also declare that I have adhered to all principles of academic honesty and integrity and have not misrepresented or fabricated or falsified any idea/data/fact/source in my submission. I understand that any violation of the above will be a cause for disciplinary action by the Institute and can also evoke penal action from the sources that have thus not been properly cited, or from whom proper permission has not been taken when needed.
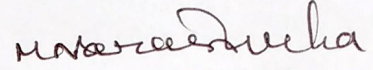
(Signature)

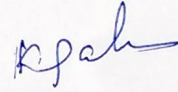KUNAL DILIP BHAGAT

(Kunal Dilip Bhagat)
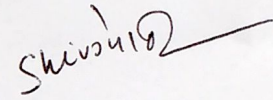
CHI4MTECH11005

(Roll No.)

Approval Sheet

This Thesis entitled Instability in pressure-driven displacement flow of one fluid by another in a pipe by Kunal Dilip Bhagat is approved for the degree of Master of Technology from IIT Hyderabad
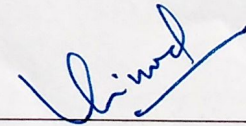
(Dr.Narasimha Mangadoddy) Examiner
Dept. of Chemical Engineering
IITH

(Dr.Kirti Chandra Sahu) Adviser
Dept. of Chemical Engineering
IITH

(Dr.Shiv Govind Singh) Co-Adviser
Dept. of Electrical Engineering
IITH

(Dr Vinod Janardhanan) Chairman
Dept. of Chemical Engineering
IITH

Acknowledgements

It is my proud privilege to express my heartful gratitude and intense thanks to Dr.Kirti Chandra Sahu, my project guide for his constant encouragement and prolific ideas, which has brought my Masters successfully to completion. I also thank him for allowing me to do project under his guidance. I learnt many things from him during the duration of my project. I owe him for this throughout my life.

I sincerely express my gratitude to my co-adviser Dr. Shiv Govind Singh, Department of Electrical Engineering and the Nano Lab staff of IIT Hyderabad for helping me whenever I needed them. Their suggestions were always useful to me.

I record my acknowledgement to Premlata(Ph.D scholar,IIT-H), Dr.Manoj Kumar Tripathi and my Multiphase flow & Fuel cell lab friends. I also like to thank P.V. Prakash, my room-mate with whom I used to constantly discuss about various ideas/techniques related to project and also was a constant support for this entire period.

I am equally indebted to my parents, for their constant support, encouragement and the moral support they gave me throughout my work.

Dedication

To my Family and the Lord Almighty

Abstract

The pressure-driven displacement flow of one fluid by another has been widely studied in literature due to its relevance in many natural phenomena and industrial applications, such as pumping of crude oil, in food processing industry, in enhanced oil recovery, to name a few. The present thesis consists of two parts. In the first part, pressure-driven displacement flow of a less viscous fluid initially occupying an axisymmetric pipe by a highly viscous fluid is investigated by conducting numerical simulations. The fluids consist of two species diffusing at different rates. The fluids are assumed to be Newtonian, incompressible with the same density, but different viscosity modelled as an exponential function of the concentration of both the species. A parametric study investigating the effects of diffusivity ratio, log-mobility ratios of the slower and faster diffusing species and Reynolds number on the flow dynamics is conducted. Our results demonstrate the presence of instability patterns due to double-diffusive effect in situations when a less viscous fluid displaces a highly viscous fluid. These instabilities are qualitatively different from those observed in planar channel. The intensity of these instabilities increases with increasing the values of diffusivity ratio. It is demonstrated that a highly viscous stenosis region is created near the entrance of the pipe due to double-diffusive effect, providing a favourable condition to start the instability. In addition to this, because of double-diffusive effect locally at some portion of the pipe, the less viscous fluid becomes the displacing fluid, which promotes the development of instability.

The second part is experimental investigation of instability in a pressure-driven displacement flow of two immiscible liquids in pipe of diameter of the order of millimetre. In this study, the pressure-driven immiscible displacement flow, focusing on the situations, where the invading fluid is less viscous than the resident fluid, is investigated experimentally in pipes of four different diameters. An extensive study has been conducted and influence of Reynolds number and capillary diameter on the flow dynamics have been investigated. The results demonstrate the presence of instability patterns due to competition between imposed pressure gradient, gravity and surface tension forces.

Contents

List of Figures

Chapter 1

Overview

The dynamics of flow of two fluids, having different viscosity and density is an interesting subject due to its relevance in many natural and industrial applications. In industries, transportation of oil and gas in pipelines [1], cooling of nuclear power station, combustion of fuel sprays in internal combustion engines and enhanced oil recovery are some of examples, wherein we encounter multiphase flows. The two-phase flow has been studied by several authors in different configurations by considering both miscible and immiscible fluids [1, 4, 5, 6, 8, 26]. The effects of geometry, density and viscosity ratios between the fluids, flow rate, surface tension have been investigated [1, 5, 6, 2, 10, 3, 20, 21, 22, 28].

1.1 Outline of the thesis

The main objective of the present study is to investigate the flow dynamics and instabilities formed in pressure-driven displacement flows of two miscible/immiscible liquids with varying viscosity, capillary diameter, diffusivity ratio and flow rate in three-dimensional geometries by performing numerical simulations and experiments.

The thesis is divided into two parts. The first part is numerical investigation of pressure-driven displacement flow of a less viscous fluid initially occupying in an axisymmetric pipe by a highly viscous fluid. The working fluids consist of two species, which are diffusing at different rates. The fluids are assumed to be Newtonian, incompressible having the same density, but different viscosity. This viscosity is modelled as an exponential function of the concentrations of both the species. A parametric study investigating the effects of diffusivity ratio, log-mobility ratios of the slower and faster diffusing species and Reynolds number on the flow dynamics is conducted. The results demonstrate the presence of instability patterns due to double-diffusive (DD) effect in situations when a less viscous fluid displaces a highly viscous fluid. It is demonstrated that a highly viscous stenosis region is formed near the entrance of the pipe due to double-diffusive effect, providing a favourable condition to start the instability.

The second part is experimental investigation of instability in pressure-driven displacement flow of two immiscible liquids in a capillary. In this study, the pressure-driven immiscible displacement flow, focusing on the situations, where the invading fluid is less viscous than the resident fluid, is investigated experimentally in pipes of four different capillary diameters. The fluids considered here are water and coconut-oil with viscosity ratio, $\mu_{21} = 27$ and density ratio, $\rho_{21} = 0.925$. An extensive

study has been conducted and the influence of Reynolds number and capillary diameter on the flow dynamics have been investigated. The results demonstrate the presence of instability patterns due to competition between the imposed pressure gradient, gravity and surface tension forces. By keeping the other parameters constant and changing the capillary diameter of the pipe changes the critical Reynolds number (Re at which the first instability formation is observed). As the Reynolds number is decreased below the Re_c, plug flow displacement behaviour is seen in the system. In this, instability phenomenon was not continuous and multiple formation of plugs are observed. Decreasing the As the capillary diameter is decreased, more axisymmetric nature of instability is observed .

Chapter 2

Instability due to double-diffusive phenomenon in pressure-driven displacement flow of one fluid by another in an axisymmetric pipe

2.1 Background

The viscous fingering phenomenon in the displacement flows of a highly viscous fluid by a less viscous one has been widely studied in literature due to its relevance in many industrial applications and natural phenomena [1]. It is also well known that the opposite situation, wherein a less viscous fluid is displaced by a highly viscous one is stable [4, 5, 6, 2, 3]. However, these conclusions are only true for single-component" systems, where viscosity stratification is achieved by varying one species, say temperature or concentration. Recently, it was observed that the classically stable viscosity-stratified configurations in the context of single-component flows become unstable in the presence of two species having different diffusion constants (say, temperature and salt, or sugar and salt, etc) in porous media [7], and pressure-driven flows in two-dimensional planar channel [9, 8, 10, 11, 12, 13]. This phenomenon is commonly known as double-diffusive effect, which has been extensively studied in density-stratified systems (see for example Turner [14]), but has received far less attention in viscosity-stratified flows. Moreover, to the best of our knowledge, all the previous studies are conducted for planar geometries, although in most of the industrial applications the geometries are circular in cross section. The flow dynamics in a circular pipe are very different to those of the planar channel, as far as the instability and transition to turbulence are concerned [15]. Thus, the focus of the present study is to investigate the instability patterns due to the double-diffusion phenomenon in an axisymmetric pipe. The double-diffusive phenomenon observed in density-stratified systems in the context of thermohaline convection is briefly discussed below [16].

The viscosity-stratified single-component systems have been studied by many authors [26, 20, 21, 22, 17, 18, 19, 23, 24, 25]. Several configurations, such as core-annular, three-layer and displacement flows are considered in these studies. The relevant finding from these studies are summarized as

follows. In three-layer planar channel flow, decreasing the viscosity towards the wall has a significant stabilizing influence. As expected, the stabilizing effects accentuated with the decrease in viscosity contrast of the fluids occupying the near-wall and centreline regions. On the other hand, increasing the viscosity of the fluid toward the walls destabilizes the three-layer channel flow. In such unstable configurations, Sahu et al. [24] found the presence of absolute instability under certain parameter ranges by conducting a linear stability analysis, which in turn takes the flow towards a transitional state via non-linear mechanism. On the other hand, core-annular pipe flow is different. For higher viscosity ratios, the flow becomes unstable even when the less-viscous fluid is at the wall [22]. By conducting a linear stability analysis, Govindarajan and co-workers [9, 10] observed a new instability mode due to double-diffusive phenomenon in a three-layer planar channel flow with the less viscous fluid occupying the near wall regions. The mixing in single-component viscosity-stratified flow in porous media has been investigated by Jha et al. [28, 27]. The readers are referred to the recent review articles [6, 11], which discuss the instability in viscosity stratified flows.

As the above brief review shows, all the previous work carried out on double-diffusive effect has so far been for planar channel, although cylindrical geometries are frequently encountered in industrial applications. The present study is an extension of Mishra et al. [9] and Sahu [8] to investigate the double-diffusive effect for displacement flow through an axisymmetric pipe. Through a series of direct numerical simulations, they investigated the instabilities due to double-diffusive effect in pressure-driven displacement flow of a less viscous fluid by a highly viscous fluid, which is injected at the inlet of a planar channel. As discussed above this is a stable configuration in the context of single-component flows. The effects of diffusivity ratio of the faster and slower diffusing species have been investigated and various instability patterns were found once the finger of the highly viscous fluid penetrates inside the channel.

The rest of this study is organized as follows. The formulation and equations governing the flow are presented in section 2.2. The results are discussed in section 2.3. Concluding remarks are given in section 2.4.

2.2 Formulation

We consider pressure-driven displacement flow of one fluid (fluid 2) by another one (fluid 1) in an axisymmetric pipe of diameter D and length L, as shown in Fig. 2.1. Both the fluids have the same density, and are assumed to be incompressible and Newtonian, with dynamic viscosities μ_1 and μ_2, respectively. The viscosity of the invading fluid is higher than that of the resident fluid ($\mu_1 > \mu_2$). This is a stable configuration in the context of single-component systems [3, 6], as discussed in section 2.1. Here, the resident (fluid 2) and invading (fluid 1) fluids consist of the same solvent, but contain two species (S and F) diffusing at different rates, wherein S and F represent the slower and faster diffusing species, respectively. D_f and D_s are the diffusivities of the faster and slower diffusing species, respectively, such that $\delta = D_f/D_s > 1$ (by definition). The pipe wall is assumed to be rigid and impermeable, with inlet and outlet at $x = 0$ and $x = L$, respectively. In order to minimize the entry effects, at the starting of the simulation the invading fluid is filled up to $x = D$ inside the pipe. The invading fluid (fluid 1 having species S and F in quantity S_1 and F_1) is injected at the inlet of the pipe with an average velocity, V ($\equiv$ Q/A), where Q and A ($\equiv \pi D^2/4$) denote the flow rate and cross-sectional area of the pipe, respectively. The resident fluid (fluid 2 having species
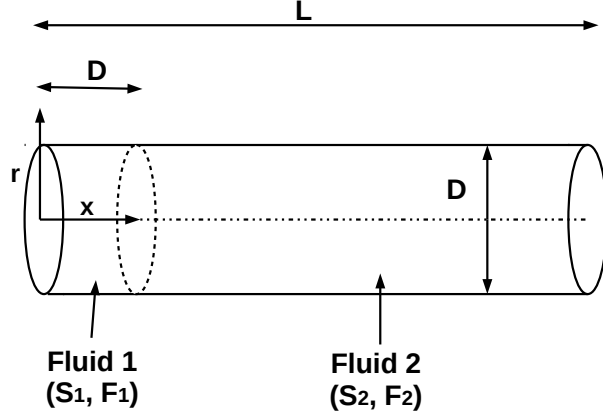
Figure 2.1: The schematic (not to scale) showing the initial flow configuration. The portions of the pipe $0 \leq x \leq D$ and $D \leq x \leq L$ are filled with fluid 1 and fluid 2, respectively. The aspect ratio of the pipe, L/D is 100.

S and F in quantity S_2 and F_2) is initially kept stationary inside the pipe $(D \leq x \leq L)$. The length of the pipe is considered to be 100D. The viscosity, μ is modelled using the following viscosity-concentration relationship [4, 10, 29, ?] for liquid systems:

$$\mu = \mu_1 exp \left[R_s \left(\frac{S - S_1}{S_2 - S_1} \right) + R_f \left(\frac{F - F_1}{F_2 - F_1} \right) \right] \tag{2.1}$$

where $R_s \equiv (S_2 - S_1)(d(ln\mu)/dS)$ and $R_f \equiv (F_2 - F_1)(d(ln\mu)dF)$ are the log-mobility ratios of species S and F, respectively. We have used this viscosity-concentration relationship as the objective of this study is to compare the flow dynamics with double-diffusive effects in an axisymmetric pipe with those observed in an two-dimensional channel [8, 9].

An axisymmetric cylindrical coordinate system (r, x) is used to formulate the problem, where r and x denote the radial and axial coordinates, respectively. The flow dynamics is governed by the continuity and the Navier-Stokes equations coupled to the convective-diffusion equations of both species through concentration-dependent viscosity. The following scaling is employed in order to render the governing equations dimensionless:

$(r, x) = D(\widetilde{r}, \widetilde{x}), t = \frac{D\widetilde{t}}{v}, (u, v) = v(\widetilde{u}, \widetilde{v}), P = \rho v^2 \widetilde{P}, \mu = \mu_1 \widetilde{\mu}$

$$\widetilde{S} = \frac{S - S_1}{S_2 - S_1}, \widetilde{F} = \frac{F - F_1}{F_2 - F_1} \tag{2.2}$$

where the tildes designate dimensionless quantities. After dropping tildes, the dimensionless governing equations are given by

$$\nabla \cdot \mathbf{u} = 0 \tag{2.3}$$

$$\rho \left[\frac{\partial \mathbf{u}}{\partial t} + (\mathbf{u} \cdot \nabla)\mathbf{u} \right] = -\nabla p + \frac{1}{R_e} \nabla \cdot \mu(\nabla \mathbf{u} + \nabla \mathbf{u}^{\mathbf{T}}) \tag{2.4}$$

7

$$\left[\frac{\partial s}{\partial t} + (\mathbf{u} \cdot \nabla s)\right] = \frac{1}{R_e S_c}\nabla^2 s \qquad (2.5)$$

$$\left[\frac{\partial f}{\partial t} + (\mathbf{u} \cdot \nabla f)\right] = \frac{1}{R_e S_c}\nabla^2 f \qquad (2.6)$$

where u(u, v) represents axisymmetric velocity field, wherein u and v are the velocity components in the axial and radial directions, respectively; p denotes the pressure field; t is the time. Here $Re(\equiv \rho V D/\mu_1)$ and $Sc(\equiv \mu_1/\rho D_s)$ denote Reynolds number and Schmidt number, respectively. The dimensionless viscosity has the following dependence on F and S:

$$\mu = \exp(R_s s + R_f f) \qquad (2.7)$$

such that $R_s + R_f < 0$ represents the situation considered here, where the invading fluid is more viscous than the resident fluid. By setting either $R_f = 0$, or $R_s = 0$ and $\delta = 1$, we can recover the governing equations for single component systems.

Eqs. (2.3)-(2.7) are solved using no-slip, no-penetration and no-flux conditions at the pipe wall. A fully-developed velocity profile with a constant flow rate ($u_i = (0.25 - r^2)32/\pi, v_i = 0$) is imposed at the inlet, wherein u_i and v_i denote the axial and radial velocity components at the inlet, respectively. Neumann boundary condition for pressure is used at the outlet of the pipe.

A finite-volume open source code, Gerris [31, 32] with dynamic adaptive grid refinement based on the vorticity magnitude and species concentration is used to solve Eqs. (2.3)-(2.6). A finest grid size of 0.015 (approximately) has been used for the regions which contain gradients of slower or faster diffusing species. Grids of size 0.06 (approximately) have been used to resolve the vortical regions inside the domain. We refer the readers to Tripathi et al. [32, 33, 34] for detailed description of the numerical method used in this study. The present grid size distribution was found to yield grid independent results for the onset of instability and other flow features. In order to validate our code, we have simulated displacement of one fluid by another in a two-dimensional planar channel for the same parameter values considered by Mishra et al. [9]. The spatio-temporal evolution of s contours for three values of is presented in Fig. 2.2. It can be seen that as expected $\delta = 1$ (single-component) is a stable configuration, but for $\delta > 1$ the flow becomes unstable forming Kelvin- Helmholtz (KH) type instabilities at the mixed regions. It is to be seen that these flow patterns are in agreement with those presented in Mishra et al. [9]. However, note that fluid 2 was filled completely inside the channel considered by Mishra et al. [9], whereas in the present study, we filled fluid 2 in the region $H \leq x \leq L$ of the channel in order to minimize the entry effect, where H is the height of the channel. In addition, the solver has been validated extensively for several interfacial flow problems [32, 33, 34], which have been excluded from here for brevity.

In the present study, we have extended the work of Sahu and co-workers [9, 8] to investigate the effects of double diffusion associated with the displacement flow of a less viscous fluid by a highly viscous one in an axisymmetric pipe. This is a parametrically rich problem, with several dimensionless numbers, such as Re, Sc, R_s, R_f and δ influencing the flow dynamics. The effects of these dimensionless variables are discussed below.
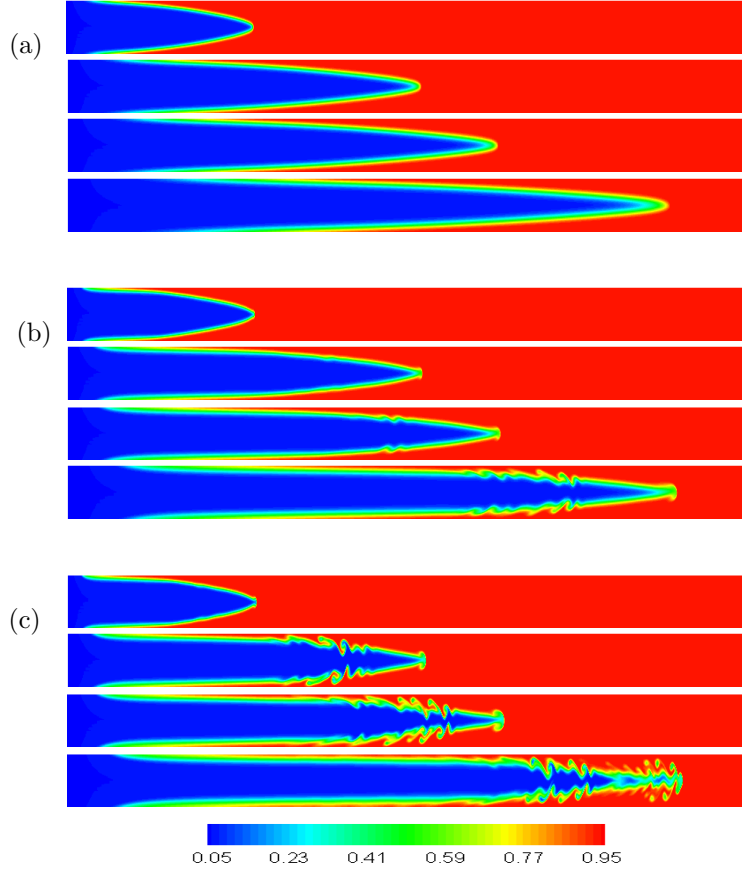
Figure 2.2: Spatio-temporal evolution of the concentration field of species s at different times in a two-dimensional planar channel (from top to bottom, $t = 20$, 30, 40, 50 and $t = 75$) for (a) $\delta = 1$, (b) $\delta = 5$ and (c) $\delta = 10$. The rest of the parameter values are $Re = 100$, $Sc_s = 100$, $Rs = 3$ and $Rf = -3.6$. The flow dynamics obtained using the present solver is very similar to those observed in Mishra et al. [9].

2.3 Results and discussion

2.3.1 Effect of δ

We begin the presentation of our results by investigating the effects of δ on the flow dynamics in Fig. 3(a)-(d), where spatio-temporal evolution of s field has been plotted for $= 1$, 2.5, 5, and 10, respectively. The rest of the parameter values used to generate this figure are $Re = 100$, $Sc = 100$, $R_s = 3$ and $R_f = 3.6$. Here $R_s + R_f < 0$, but $R_s > 0$ and $R_f < 0$, which corresponds to a situation when a highly viscous fluid displaces a less viscous fluid, and the slower and faster diffusing species have destabilizing and stabilizing influences, respectively. For instance, in this case the slower and faster diffusing species could be sugar and temperature, respectively. It can be seen that, as expected, for $\delta = 1$ the flow dynamics is stable, and a pure-Poiseuille-diffusive flow occurs as the finger penetrates inside the pipe. It can be seen that the KH type instabilities appear for $\delta > 1$. The intensity of instability increases with an increase in the value of δ. Such behaviour is testament to the ability of DD to destabilize an otherwise stable situation and for which there are several diverse

examples [7, 16]. For the regime under consideration here, we observe that $\delta \approx 2.5$ corresponds to the onset of instability, and which can be seen in the contours of s. Close inspection of Fig. 3(b) reveals that a spike like structure appears at the tip of the finger at later times ($t40$). For higher values of δ, the KH type instability becomes catastrophic. Roll-up structures become apparent at earlier times and have increasingly greater intensity as time progresses. Comparison of contours of s for $\delta = 10$ observed in an axisymmetric pipe (Fig. 3(d)) with those seen in a two-dimensional planar channel (Fig. 2(d)) divulge that the mushroom-like structures which are clearly visible in a planar channel do not appear in case of axisymmetric pipe, and the intensity of instability is greater for the case of a two-dimensional planar channel. Also DD convection affects pipe flow for much smaller value of than the channel case. It can be seen in panel (b) of Figs. 2 and 3 that the flow in a two- dimensional channel is fairly stable for $\delta = 2.5$, but the instability already appears in case of an axisymmetric pipe for the same value of δ. Close inspection of Figs. 2 and 3 also reveals that the mixing in a planar channel is dominated by instabilities, where as in a pipe it is mainly dominated by diffusion mechanism. Inspection of results presented Fig. 2 (two-dimensional channel) and Fig. 3 (axisymmetric pipe) reveals that the speed of the finger in a pipe is higher than that observed in a planar channel for the same set of parameter values. This is also evident in Fig. 4, where the time evolution of location of the tip of the finger in a two-dimensional channel and an axisymmetric pipe are presented for different values of δ. We also observed in Fig. 4 that increasing δ increases the speed of the finger for both the channel and pipe cases.

The spatio-temporal evolution of viscosity field for different values of δ is presented in Fig. 5 for the same parameter values used to generate Fig. 3. For $\delta = 1$, the viscosity in the mixed region decreases monotonically in the positive axial direction, whereas for $\delta > 1$ the viscosity undergoes a non-monotonic distribution in the axial direction due to the double-diffusive effect. In addition to this, for $\delta > 1$ a highly viscous stenosis region forms near the wall of the pipe. The value of viscosity of the fluid in the stenosis region increases with an increase in the value of δ. This phenomenon was first observed by Taylor [35] for single-component flows. The non-monotonic viscosity distribution in the axial direction and the highly viscous stenosis formation near the wall of the pipe provide a favorable condition for the instability to grow [6], leading to the amplification of instabilities for increasing values of δ.

The radial variation of viscosity at a later dimensionless time ($t = 50$) for different axial locations are plotted in Fig. 6(a)-(d) for $\delta = 1, 2.5, 5$, and 10, respectively. It can be seen that a core-annular configuration is formed with the less viscous fluid in the annular region for $\delta = 1$. The viscosity in this case decreases monotonically in the radial direction at all x locations. This is a stable configuration, as shown by Govindarajan and co-workers via linear stability analyses [6, 17]. For $\delta > 1$ the viscosity profiles encounter minima at intermediate radial locations (in the mixed region) for all axial locations, with the annular region occupied with highly viscous fluid, thus making the flow unstable. Close inspection of Fig. 6(b)-(d) also reveals that the value of the near-wall viscosity increases with an increase in δ value, thereby making the flow more unstable. The effect of the log-mobility ratio of the slower diffusing species, R_s is investigated next.

Figure 2.3: Spatio-temporal evolution of the concentration field of species s at successive times (from top to bottom, $t = 20$, 40, 50 and $t = 75$) for (a) $\delta = 1$, (b) $\delta = 2.5$, (c) $\delta = 5$ and (d) $\delta = 10$. The rest of the parameter values are $Re = 100$, $Sc_s = 100$, $Rs = 3$ and $Rf = -3.6$. The centreline of the pipe is located at the middle of each panel.

11

Figure 2.4: Spatio-temporal evolution of the viscosity field at successive times (from top to bottom, $t = 20$, 30, 40, 50 and $t = 75$) for (a) $\delta = 1$, (b) $\delta = 2.5$, (c) $\delta = 5$ and (d) $\delta = 10$. The rest of the parameter values are $Re = 100$, $Sc_s = 100$, $Rs = 3$ and $Rf = -3.6$. The centreline of the pipe is located at the middle of each panel.
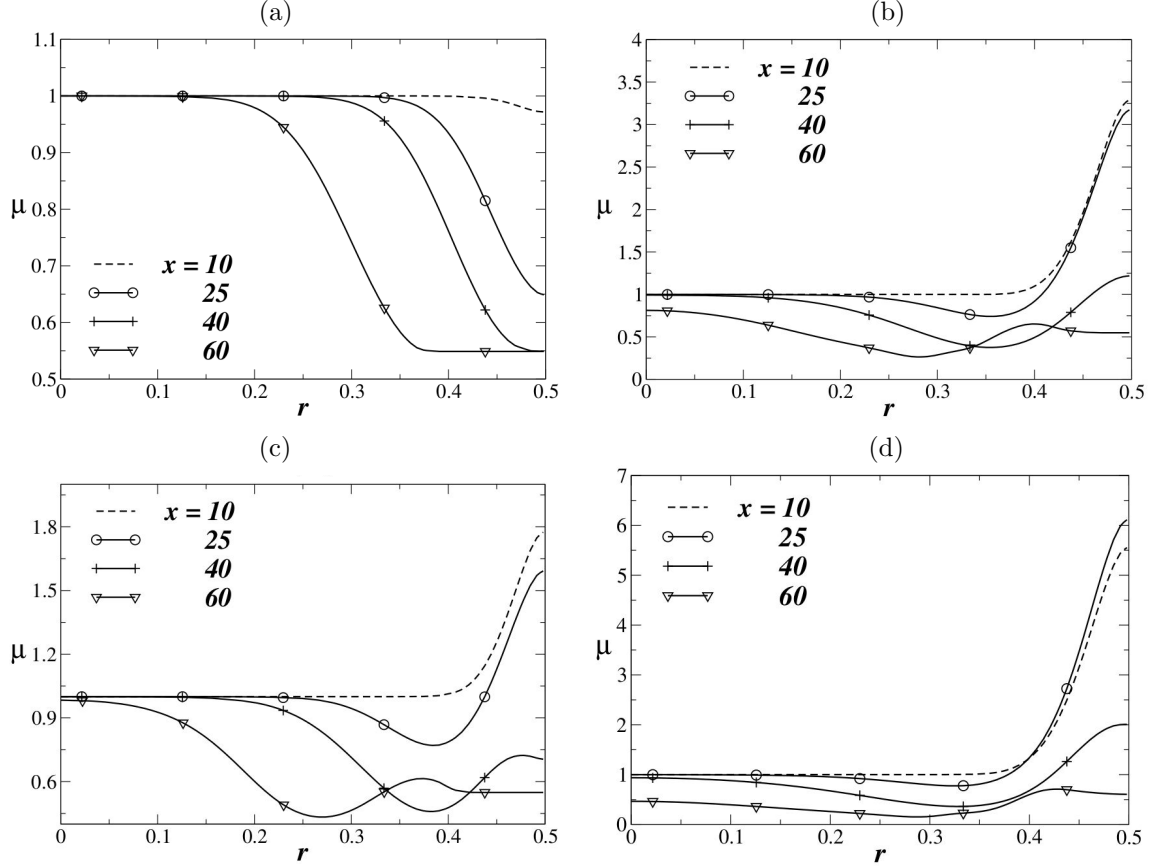
Figure 2.5: Variation of viscosity at t = 50 in the radial direction at different axial locations for (a)$\delta = 1$, (b)$\delta = 2.5$, (c)$\delta = 5$ and (d)$\delta = 10$ .The rest of the parameters are , $t = 50$, $Re = 100$, $Sc_s = 100$, $Rs = 3$ and $Rf = -3.6$.

2.3.2 Effect of R$_s$

The spatio-temporal evolutions of the concentration field of the slower diffusing species are presented for $R_s = 0.5$, 1.5, 2 and 3 in Fig. 7(a), (b), (c) and (d), respectively. The rest of the parameter values are $Re = 100$, $Sc = 100$, $\delta = 10$ and $R_f = 3.6$. Again the slower and faster diffusing species have destabilizing and stabilizing influences, respectively. In addition to this, $R_s + R_f < 0$, thus a highly viscous fluid is displacing a less viscous one inside the pipe. For $R_s = 0.5$, the viscosity of the invading fluid is approximately 22.2 times higher than that of the resident fluid. The value of δ ($\delta = 10$) considered in this case is not high enough to create instabilities. In this case, a finger with a blunt nose penetrates inside the pipe as the time progresses. With an increase in the value of R_s , the viscosity ratios between the invading and resident fluids decreases. For $R_s = 1.5$, the nose of the finger becomes sharper, and the onset of instabilities occurs at $R_s = 1.5$ for the set of parameter values considered. Further increase in the value of R_s leads to KH type instabilities at the mixed region separating the fluids. This behaviour is also evident in Figs. 8 and 9. The appearance of highly viscous stenosis region near the wall, which is the source for these instabilities is not significant enough for $R_s = 0.5$, but starts to dominate the instability dynamics for $R_s \geq 1.5$

for this set of parameter values.

The axially averaged viscosity (μ_x) versus r, and radially averaged viscosity (μ_r) versus x profiles are plotted at $t = 30$ in Fig. 9(a) and (b), respectively. It can be seen in Fig. 9(a) that for R s 1.5, the dynamics due to the double-diffusive effect creates a core-annular configuration, with highly viscous fluid in the annular region. The non-monotonic trend of the radially averaged viscosity profiles are also apparent for $R_s \geq 1.5$ in Fig. 9(b), which implies that although initially a highly viscous fluid was displacing a less viscous fluid, at later times due to the double-diffusive effects a situation is created locally, wherein a less viscous fluid displaces a highly viscous one. This phenomenon makes the flow unstable [3].
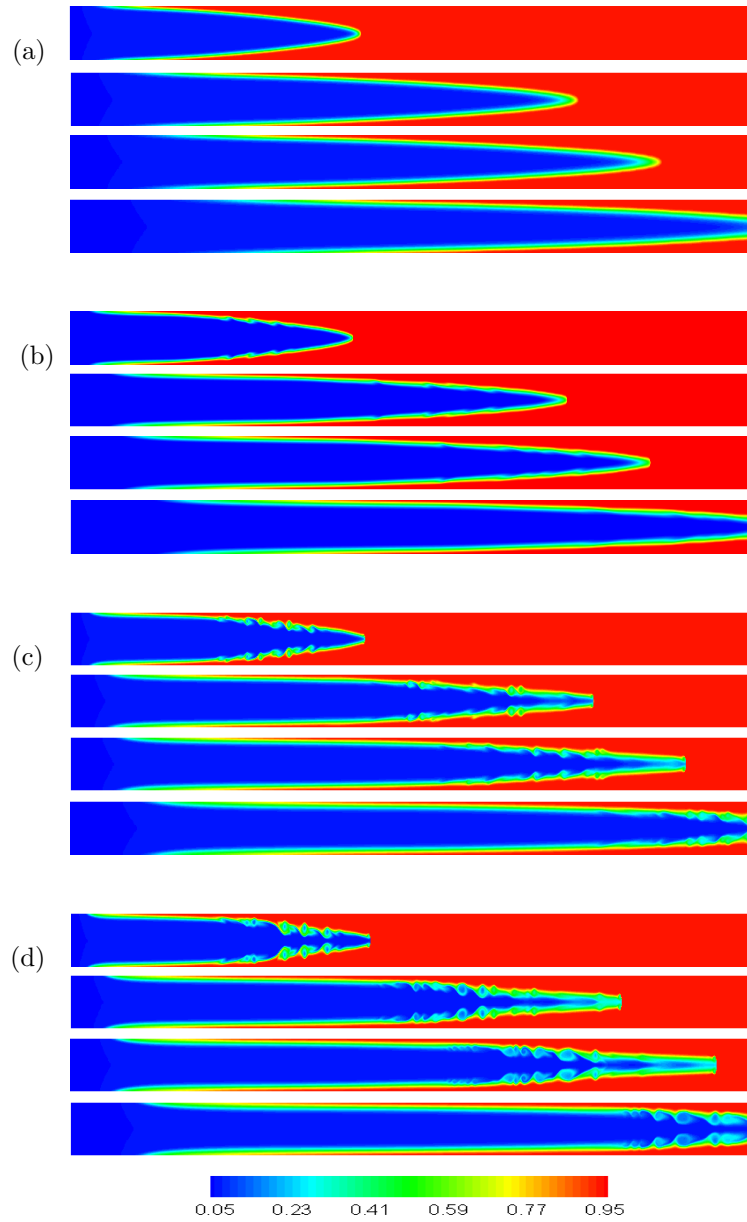

Figure 2.6: Spatio-temporal evolution of the concentration field of species s at successive times (from top to bottom, $t = 20$, 30, 40, 50 and $t = 75$) for (a) $Rs = 0.5$, (b) $Rs = 1.5$, (c)$Rs = 2$ and (d) $Rs = 3$. The rest of the parameter values are $Re = 100$, $Sc_s = 100$, $\delta = 10$ and $Rf = -3.6$. The centreline of the pipe is located at the middle of each panel.
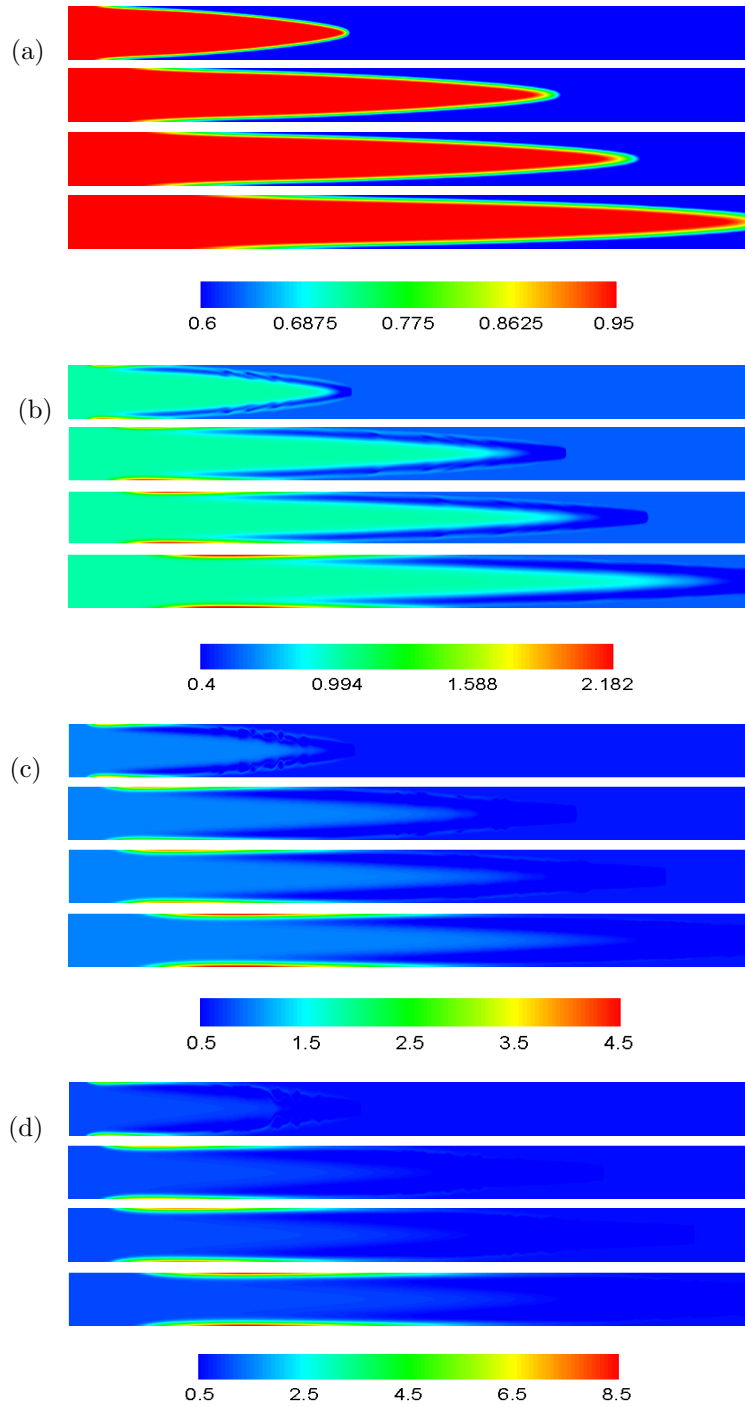
14

Figure 2.7: Spatio-temporal evolution of the viscosity field at successive times (from top to bottom, $t = 20$, 30, 40, 50 and $t = 75$) for (a) $Rs = 0.5$, (b) $Rs = 1.5$, (c)$Rs = 2$ and (d) $Rs = 3$. The rest of the parameter values are $Re = 100$, $Sc_s = 100$, $\delta = 10$ and $Rf = -3.6$. The centreline of the pipe is located at the middle of each panel.

Figure 2.8: Variation of a) axially average viscosity, ($\mu_x \equiv \frac{D}{L} \int_0^{L/D} \mu dx$) verses r, b) radially averaged viscosity ($\mu_r \equiv \frac{8}{D^2} \int_0^{D/2} \mu r dr$) verses x, for different values of R_s, at $t = 30$ for $Re = 100$, $Sc_s = 100$, $\delta = 10$ and $R_f = -3.6$.

2.3.3 Effect of R_f

We then investigate the effects of changes to the log-mobility ratio of the faster diffusing species. In Fig. 9(a), (b) and (c), we plot the spatio-temporal evolution of s for $R_f = -1$, -3 and -5 respectively. The rest of the parameter values are $Re = 100$, $Sc = 100$, $\delta = 10$ and $R_s = 2$. The results presented in Fig. 9(a) are characteristic of a situation when a less viscous fluid displaces a highly viscous fluid occupying the pipe initially (i.e. $R_s + R_f > 0$; unstable configuration even for single-component systems). It can be seen that a cap-type instability appears at the tip of the finger, with a blunt nose. The results presented in Fig. 10(b) and (c) are stable in the context of single-component systems; however, become unstable due to differential diffusivity of the slower and faster diffusing species ($\delta = 10$). Decreasing the value of R_f by keeping R_s constant decreases the double-diffusive instability. It can be seen in Fig. 10(a) that, for t=30, the viscosity contrast of the annular to the core fluids decreases with R_f. Such effect was also observed for all later times considered (not shown). Also the peak of the radially averaged viscosity near the entrance region decreases with a reduction in the value of R_f, and thereby stabilizing the flow dynamics.
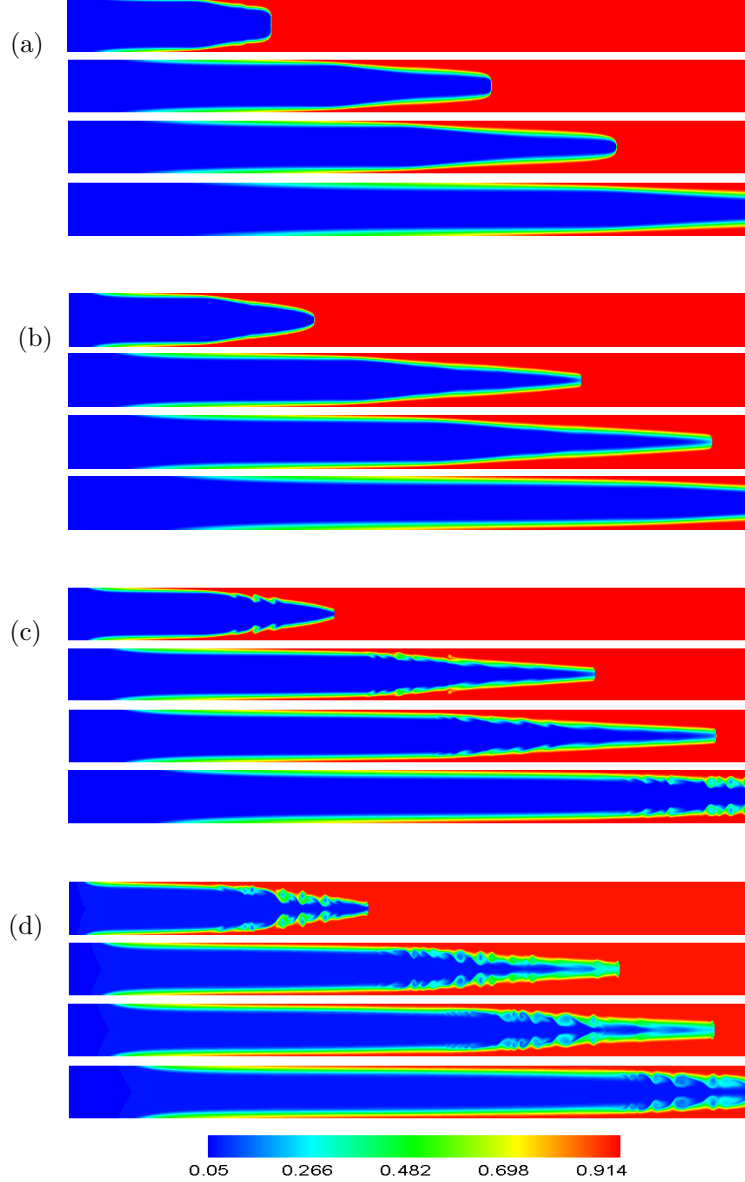

16

Figure 2.9: Spatio-temporal evolution of the concentration field of species s at successive times (from top to bottom, $t = 20$, 30, 40, 50 and $t = 75$) for (a) $R_f = -1$, (b)$R_f = -3$ and (c) $R_f = -5$. The rest of the parameter values are $Re = 100$, $Sc_s = 100$, $\delta = 10$ and $R_s = 2$. The centreline of the pipe is located at the middle of each panel.
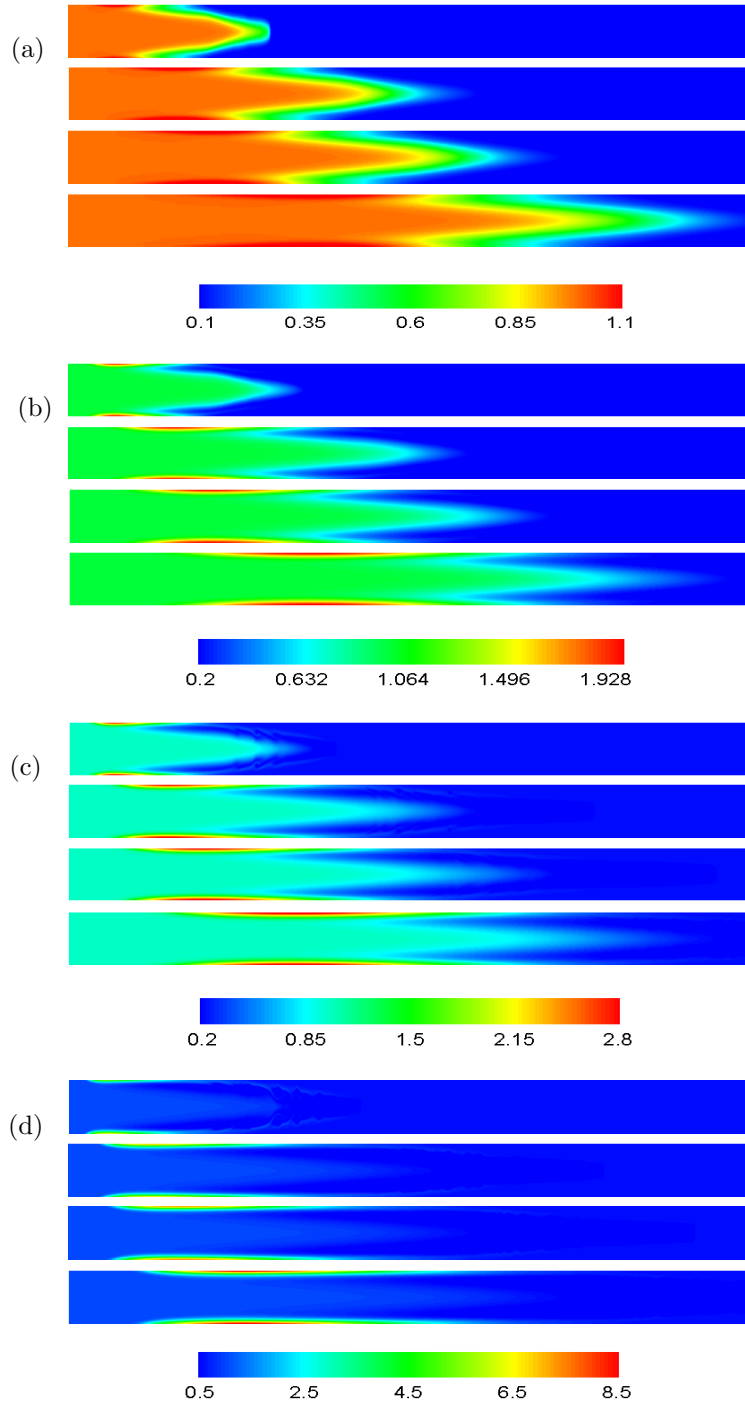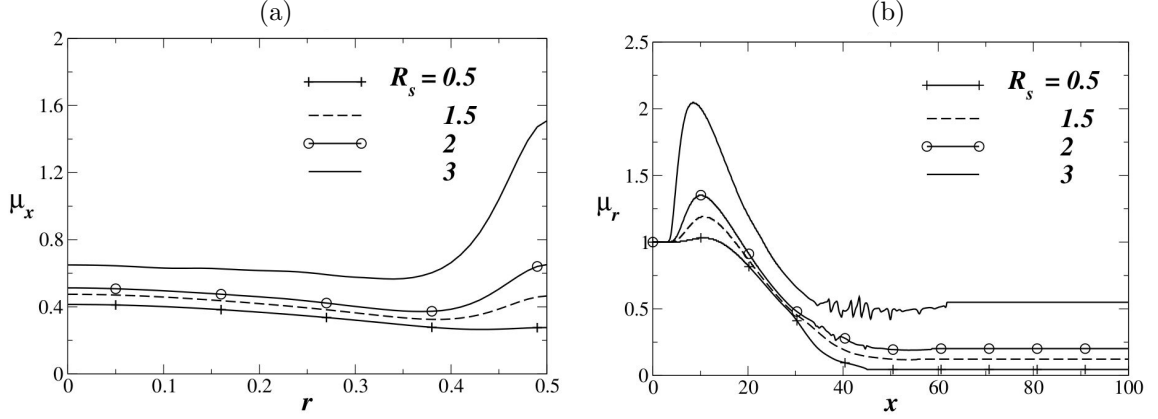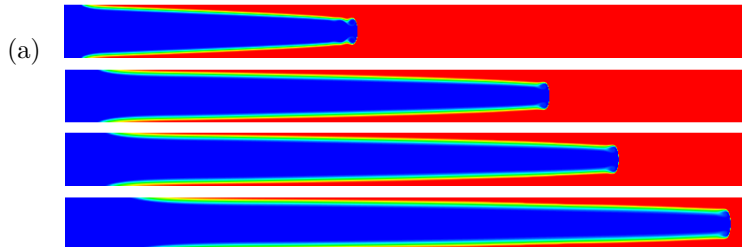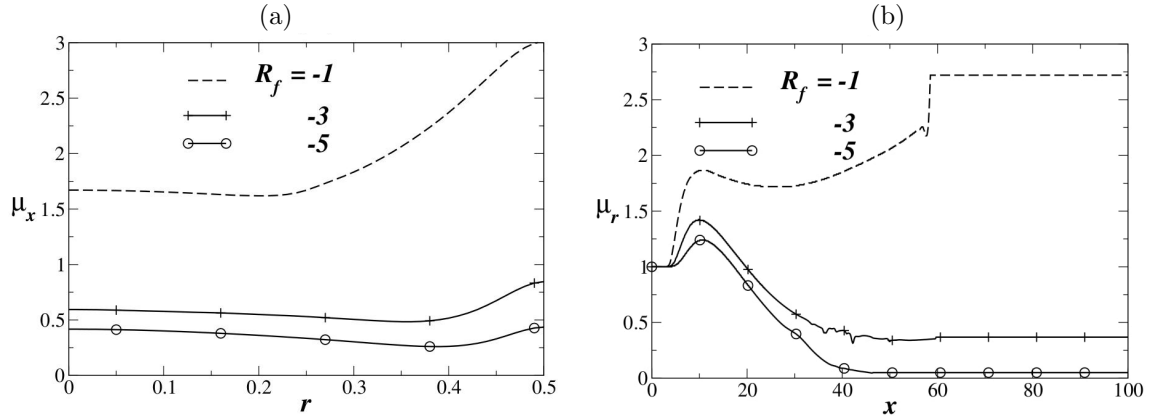

Figure 2.10: Variation of a) axially average viscosity, ($\mu_x \equiv \frac{D}{L} \int_0^{L/D} \mu dx$) verses r, b) radially averaged viscosity ($\mu_r \equiv \frac{8}{D^2} \int_0^{D/2} \mu r dr$) verses x, for different values of R_f, at $t = 30$ for $Re = 100$, $Sc_s = 100$, $\delta = 10$ and $R_s = 2$.

17

2.3.4 Effect of Re

Finally, in Fig. 2.11, the effects of Re are shown for $Sc = 100$, $\delta = 10$, $R_s = 3$, and $R_f = 3.6$. It can be seen that flow becomes vigorously unstable with an increase in the value of Re. This behaviour is not surprising as the destabilizing behaviour of Reynolds number can be observed in many shear flows. Close inspection of this figure also reveals that the nose of the finger becomes increasingly sharp as Re is increased, but surprisingly becomes blunt for $Re = 1000$. Increasing Reynolds number by keeping the Schmidt number fixed also implies that the Peclet number ($ReSc$), which characterizes diffusion, is increased. It can be seen in Fig. 2.11 that the mixing due to diffusion decreases with an increase in the value of Re, which increases (decreases) the Peclet number (diffusive mixing). Comparison of the spatio-temporal variation of s contours shown in Fig. 2.11 for an axisymmetric pipe with those of Mishra et al. [9] for a two-dimensional channel reveals that the present flow is more unstable than that observed in a channel.
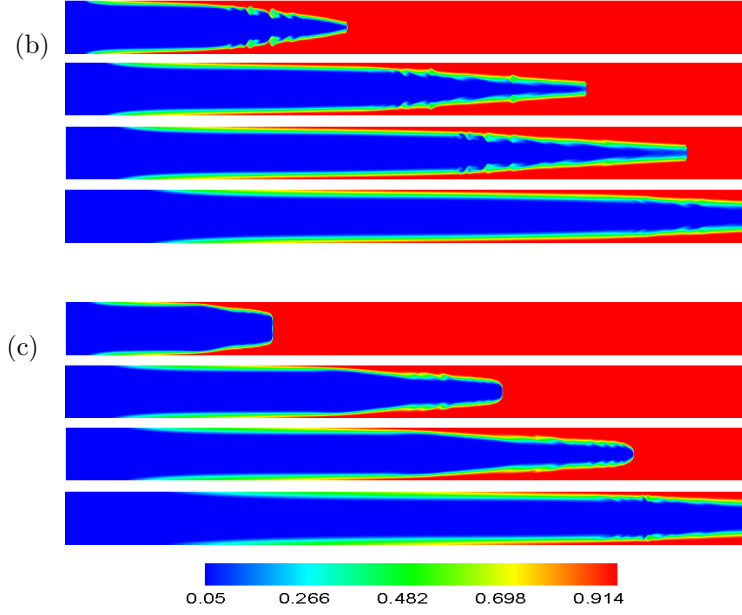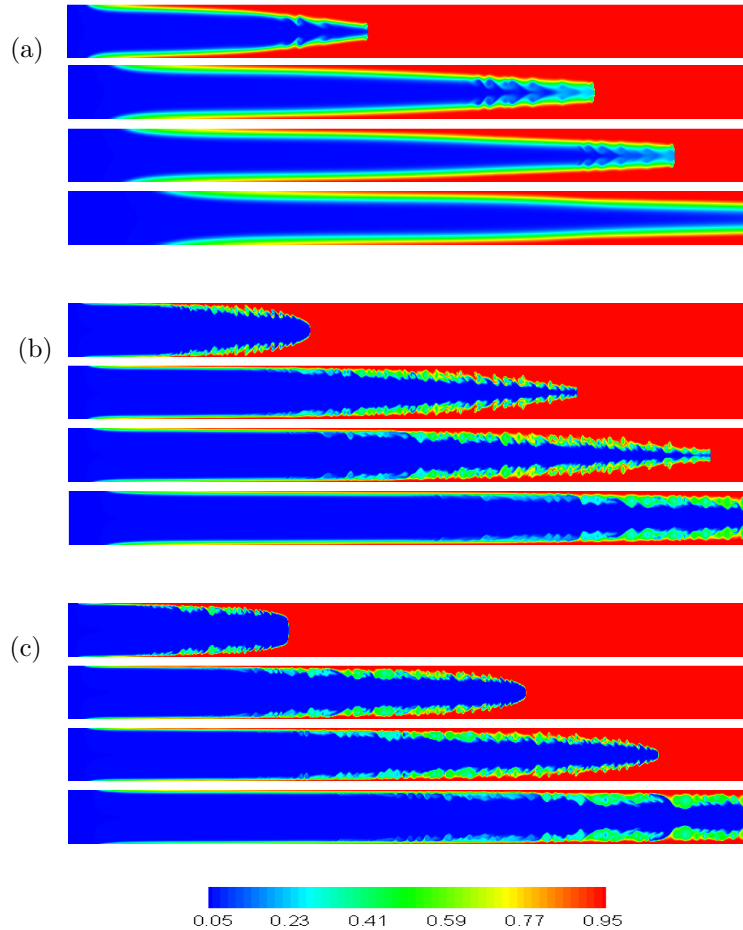

Figure 2.11: Spatio-temporal evolution of the concentration field of species s at successive times (from top to bottom, $t = 20, 30, 40, 50$ and $t = 75$) for (a) Re = 50, (b) Re = 500 and (c) Re = 1000. The rest of the parameter values are $Sc_s = 100$, $\delta = 10$ $Rs = 3$ and $Rf = -3.6..$ The centreline of the pipe is located at the middle of each panel.

18

2.4   Concluding remarks

In this paper, the pressure-driven displacement flow, focusing on the situation when the invading fluid is more viscous than the resident fluid (classically a stable configuration in the context of single-component systems), is investigated in an axisymmetric pipe, using an open source code, Gerris based on finite-volume approach. The fluids considered in the present study have the same density, but different viscosity. The viscosity stratification is achieved through the addition of two solute species diffusing at different rates. The viscosity is modelled as an exponential function of the concentration of both the species. An extensive parametric study has been conducted, and the influences of diffusivity ratio, log-mobility ratios of the slower and faster diffusing species, and Reynolds number on the flow dynamics have been investigated. Our results demonstrate the presence of instability patterns due to double-diffusive effect, which are qualitatively different from those observed in a planar channel and also in situations when a less viscous fluid displaces a highly viscous fluid. We found that increasing the values of δ and R_s, keeping R_f fixed, makes the flow increasingly unstable. Similar trend is observed when the Reynolds number is increased. We observe a blunt nose of the penetrating finger for lower value of R_s, which becomes sharper with increasing R_s value. It is demonstrated that although initially a highly viscous fluid displaces a less viscous one, at later times, a local situation is created due to the double-diffusive phenomenon, wherein less viscous fluid becomes the displacing fluid. Also, at later times, the viscosity of the fluid in annular region becomes more viscous as compared to that in the core of the pipe, which starts the instability observed in the present study.

Chapter 3

An experimental study of instability in pressure-driven displacement flow of two immiscible liquids in capillary tubes

3.1 Background

As discussed in the previous chapter, in pressure-driven displacement flow of a less viscous fluid by a more viscous fluid, the interface separating the two fluids becomes unstable. When the fluids are immiscible, the Yih type instability [36] appears at the interface, whereas the Kelvin-Helmoltz-type roll-up structures form at the so called 'interface' of two miscible fluids. In miscible/immiscible flow configurations, several numerical and experimental studies have been carried to understand the flow dynamics, which is reviewed recently by Govindarajan and Sahu [6]. Sahu et al. [37] numerically investigated the three-dimensional displacement flow of a liquid originally occupying a square duct by another immiscible liquid of different density and viscosity, which is injected from the inlet of the channel. The effect of viscosity ratio, density ratio, surface tension, wettability and capillary number was also studied by Chin et al. [38], Grosfils et al. [39], Kang et al. [40], and Dong et al. [41], respectively. In this chapter, displacement flow of coconut oil organically occupying inside a pipe by water is investigated experimentally. An parametric study has been conducted and the influence of Reynolds number and capillary diameter on the flow dynamics have been investigated. The results demonstrate the presence of instability patterns due to competition between imposed pressure gradient, gravity and surface tension forces.

3.2 Experimental set-up and procedure

The experimental set-up of pressure-driven displacement flow of one fluid by another immiscible fluid in a capillary tube is shown in Fig 3.1. The set-up consists of glass capillaries with nominal inner diameters, D = 0.5, 1, 2 and 3 mm. The capillary tubes were mounted on a glass holder stand, made up of iron, so as to avoid any disturbance/vibrations during the experiment. Initially the capillary was filled with coconut oil (fluid 2) with dynamic viscosity, $\mu_2 = 27$ cp and density, $\rho_2 = 925 \ kg/m^3$. One end of the capillary was connected to a micro-pump and the other end was kept open to atmospheric conditions. A syringe of 30 ml was mounted on the micro-pump which contained water (fluid 1) with dynamic viscosity $\mu_1 = 1$ cp and density $\rho_1 = 1000 \ kg/m^3$. Water was coloured pink with $KMnO_4$ to capture the water-coconut oil interface through the glass capillary tubes. Water was injected into the capillary tubes with different volumetric flow rates (0.5 - 30 ml/min). A scale was attached to the iron stand to track the location of finger-tip and instabilities along the capillary tube length. A digital camera was used to capture the instability phenomena for a certain length of the capillary. Experiments were repeated for various volumetric flow rates to calculate the error bar related to displacement of finger tip and instabilities. It was found that the error related to the finger tip and instability displacement was ±3% and ±1.2%, respectively (Figs. 3.4-3.5).

Experiments were performed to obtain the value of contact angle for water and coconut-oil with glass for account of surface tension. The contact angles at water-air (θ_w) and coconut oil-air (θ_c) junctions at the tube wall were found to be 18^0 and 55.6^0, respectively. The interfacial tension between the water and coconut-oil interface is 12.8 mN/m^2 [42]. Both the fluid tends to wet the surface of the glass tube and this wetting properties has a profound influence on the width of the penetrating fluid and consequently on the shape of the overall pattern [43].

Image processing techniques was used on the images collected from the digital camera to extract the desired data [44]. This was basically done using Matlab image processing toolbox. Initially the images are cropped such that only tube part is visible (Fig. 3.3). The resulting image is then converted into grayscale by the Matlab functions. Intensity versus x diagram is obtained by averaging the intensity values of each column. A threshold value of 115 is taken to obtain the peaks in the intensity versus x diagram (not shown). The peaks are tracked with time to obtain the motion of the thin regions of the pink fluid (water). The motion of finger tip at different times are plotted (Fig.3.4-3.5) for different Re.

The influences of Reynolds number(Re) and capillary diameter(Ca_d) on the flow dynamics are discussed below.
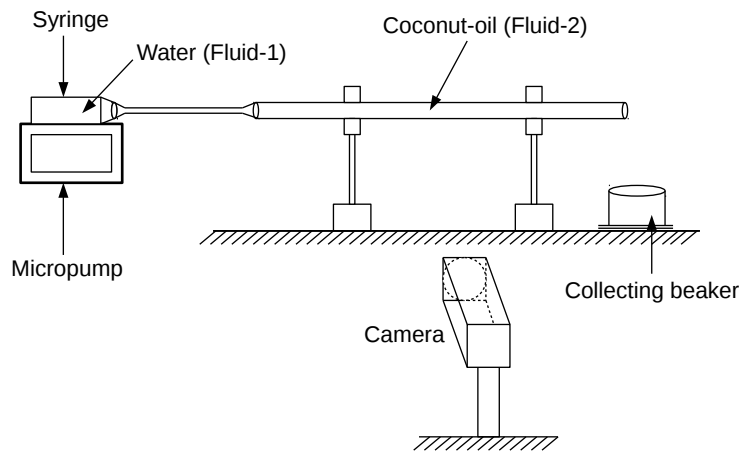
Figure 3.1: A schematic of the experimental set-up for the pressure-driven immiscible displacement of one fluid by another in a capillary.
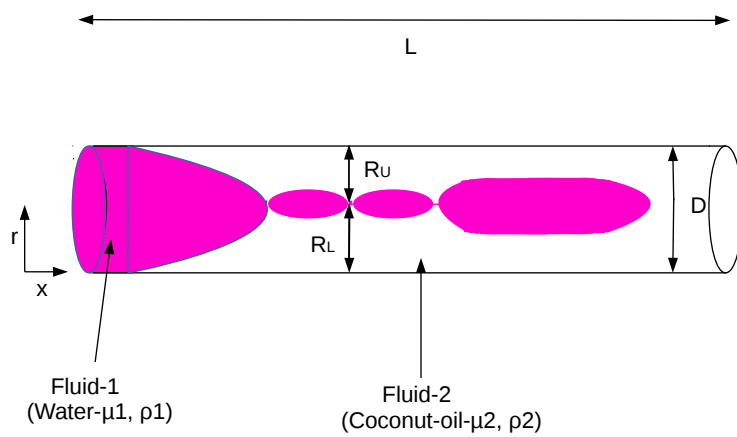

Figure 3.2: A schematic of water displacing coconut-oil in a capillary.

3.3 Results and discussion

3.3.1 Effect of Re

We now begin our analysis by investigating the effect of Re (Reynolds number) which introduces instability in the system. In the present study, experiments were carried out for Re ranging from $40 - 300$ for all the four capillary tubes. The effect of Re on the flow dynamics is presented in the current section where all other parameters are kept constant and only volumetric flow rate is varied in each capillary tube. In the present section, the study includes finger-tip tracking, instability tracking by image processing techniques and identification of a critical Reynolds number Re_c, at which the first instability formation in the system was observed. As the Reynolds number is decreased below the Re_c, plug flow displacement behaviour was seen in the system (Fig 3.3(a)). In this, instability phenomenon (Neck-Break formation) was not continuous and multiple formation of plugs ware observed below the Re_c value.

The effect of Re on the flow dynamics is shown in Fig 3.3(a)-(d), where spatio-temporal evolution of the concentration field of water has been plotted for Re = 72, 83, 120 and 180 respectively. The rest of the parameter values are, Ca_d = 2mm, L = 10cm, μ_1 = 1cp, μ_2 = 27cp, $\rho_1 = 1000kg/m^3$ and $\rho_2 = 925kg/m^3$. The Re is calculated based on the fluid 1 (water) and defined as $Re = DV\rho_1/\mu_1$, where the Ca_d = diameter of the capillary, V = Velocity of the fluid 1 injected, ρ_1 = density of fluid 1 and μ_1 = viscosity of fluid 1. Here $\mu_2 > \mu_1$ which corresponds to a situation when a less viscous fluid displaces a highly viscous fluid and hence is an unstable system [1]. In Fig 3.3(b)-(d), for Re $\geq Re_c$, it can be seen that the instability formation is continuous and no plug flow displacement occurs as the finger penetrates inside the capillary tube. For this set of parameter values, we observe that $Re = 83$ corresponds to the critical Reynolds number for which the initial instability is seen (Fig 3.3(b)). Similarly, the Re_c values for capillary diameter $Ca_d = 0.5$, 1 and 3mm was found to be 95, 48 and 120 respectively (Fig 3.8). Close inspection of Fig 3.3(b)-(d) reveals that, initially the instabilities are waves in structure [45] and as the finger penetrates inside the capillary, kink type instability is observed [46]. This kink type pattern can be seen in Fig 3.3(b)-(d), and termed in this study as "Neck-break formation" (N-B). It is observed that the intensity of the instability increases as the Reynolds number is increased. This destabilizing behaviour of Reynolds number can be observed in many shear flows [6]. In the initial stages, the N-B type instability is seen to form at the tails end and as the Re is increased further, simultaneous N-B type instability formation is seen in the whole capillary tube.

The variation of the location of finger-tip (X_{tip}) at different time interval for capillary diameter D = 0.5, 1, 2 and 3mm and $20 \leq Re \leq 300$ is presented in Fig 3.4(a)-(d), for same parameter values used in Fig 3.3. For this set of parameters, the ratio of single phase water velocity to finger-tip velocity (V_{sp}/V_{tip}, calculated from Fig 3.4) was found to be around 1.66 for all the capillary diameters. An error bar was plotted shown in Fig 3.4(a)-(d), which was generated by carrying out a single experiment several times.The percentage error limit for the X_{tip} in the capillary tubes was found to be ±3%. This percentage error limits were nearly same for different Reynolds number and capillary diameters (Fig 3.4). The finger-tip speed was also seen to behave different when the Re number was increased higher. In this there was a phenomenon of two N-B type merging with each other to form a new N-B type instability because of which the X_{tip} location was seen to oscillate in the capillary domain. This behaviour was seen for Re ranging from $Re_c \leq Re \leq 200$. For $Re > 200$,

the N-B type instability merging was seen faster and the finger-tip oscillations was minimized.

Now we see the effect of Re on the N-B type instability formation. The variation of location of instability (X_{int}) with respect to time for capillary diameter $Ca_d = 0.5$, 1, 2 and 3 mm and for $40 \leq Re \leq 300$ has been plotted in Fig 3.5(a)-(d). The rest of the parameter values are, $\mu_1 = 1$cp, $\mu_2 = 27$cp, $\rho_1 = 1000kg/m^3$ and $\rho_2 = 925kg/m^3$. The ratio of single-phase velocity to the instability velocity (V_{sp}/V_{int}) was found to be nearly 20.22 for all the capillary diameters.
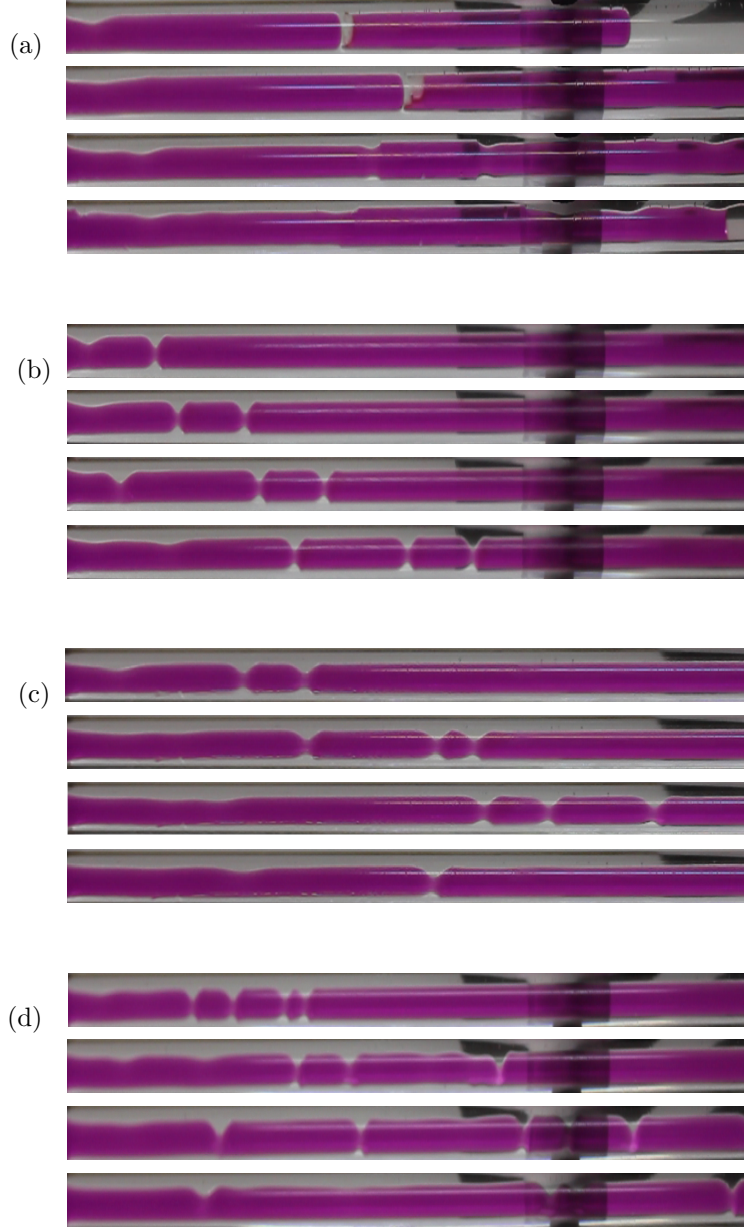

Figure 3.3: Experimental images of water penetrating inside the capillary at successive times (from top to bottom, $t = 10$, 20, 30 and $t = 50$) for Reynolds number (a) $Re = 72$, (b) $Re_c = 83$, (c) $Re = 120$ and (d) $Re = 180$. The rest of the parameters values are, D = 2mm, L = 10cm, $\mu_1 = 1$cp, $\mu_2 = 30$cp, $\rho_1 = 1000kg/m^3$ and $\rho_2 = 925kg/m^3$.
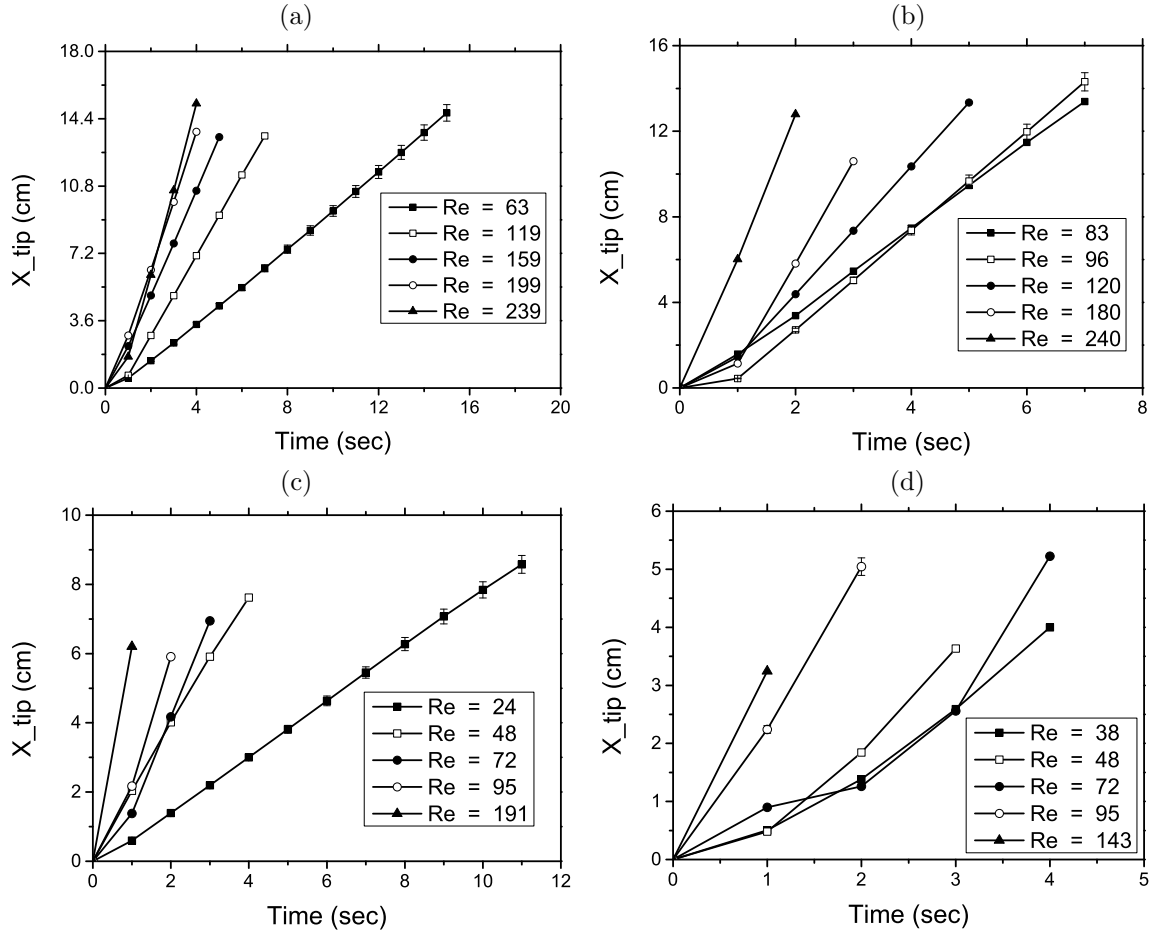
Figure 3.4: Variation of location of finger tip , X_{tip} (cm), in the steamwise direction for (a) $D = 3$mm , (b) $D = 2$mm, (c) $D = 1$mm and (d) $D = 0.5$mm .The rest of the parameters are $0 \leq t \leq 50$ sec, $0 \leq Re \leq 300$ and Aspect ratio = 1 : 100.

The observed flow dynamics (Fig 3.3) is a result of competition between the imposed pressure-gradient, surface tension force and the gravity. The pressure-driven flow induces motion of fluid 1 in positive axial direction, and the gravity acting perpendicular to flow, opposes the motion. The density difference of 7.5% was seen to affect the flow dynamics when the capillary diameter (Ca_d) was greater than 1mm. For $Ca_d \geq 1mm$, the gravity is also a dominating force acting in the downward direction settles the remnants of fluid "1" at the bottom part of the capillary tube [47]. The upper layer of the capillary tube for t $\geq$ 10 sec was thicker compared to the bottom layer (Fig 3.3 and 3.7). Interesting to observe in the flow dynamics was, the speed of the N-B type instability was much smaller as compared to the V_{tip} and V_{sp}. As we go near the bottom wall, the velocity of flow dynamics decreases due to no-slip condition and as the instability formation was seen near the bottom wall region, the velocity of instability was also seen less as compared to other flow velocity.

In $1mm$ and $0.5mm$ capillary diameter, the upper layer of coconut-oil was thin for t $\geq$ 10 sec as compared to $2mm$ and $3mm$ capillary diameter. As the finger penetrates inside the capillary tube
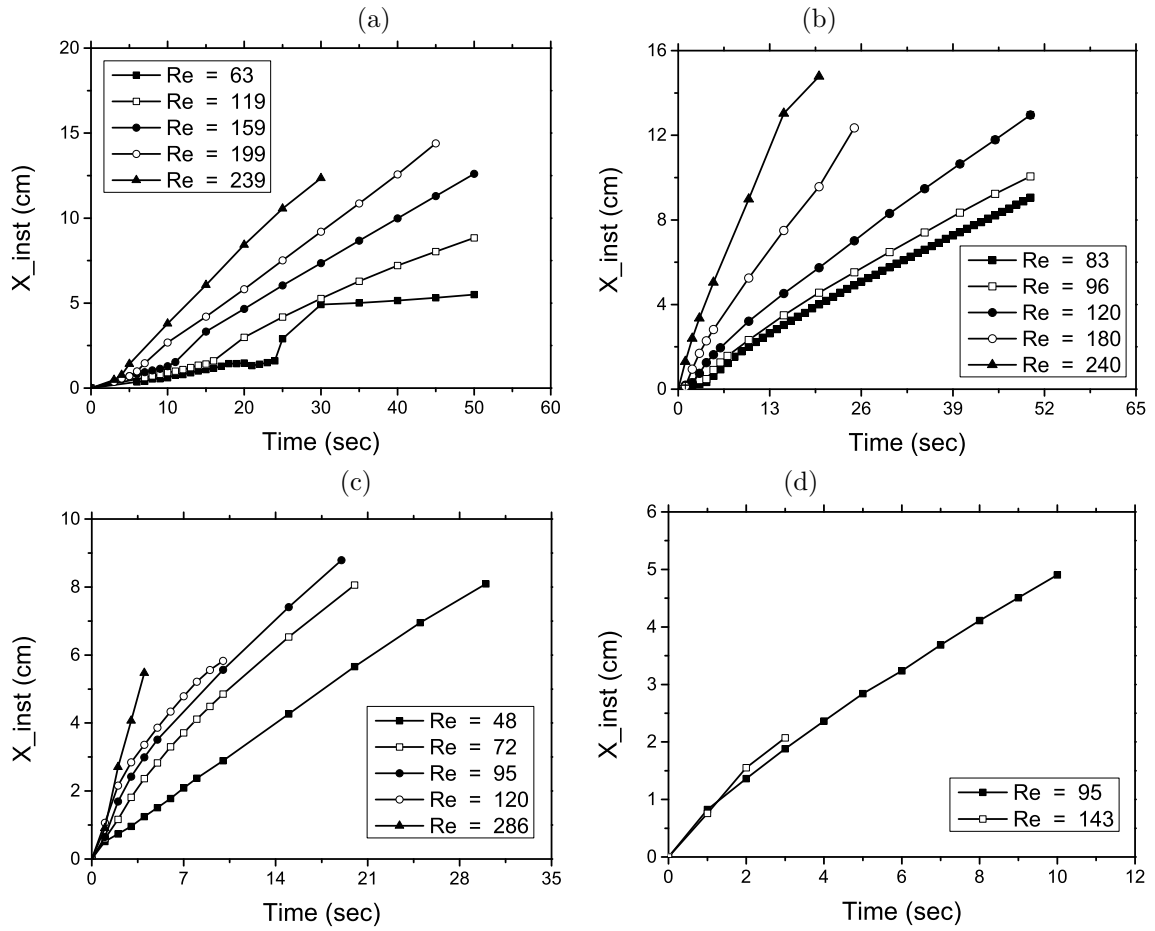
Figure 3.5: Variation of X_{int}, in the steamwise direction for (a) $Ca_d = 3$mm , (b) $Ca_d = 2$mm, (c) $Ca_d = 1$mm and (d) $Ca_d = 0.5$mm .The rest of the parameters are $0 \leq t \leq 50$ sec, $0 \leq Re \leq 300$ and Aspect ratio $= 1 : 100$.
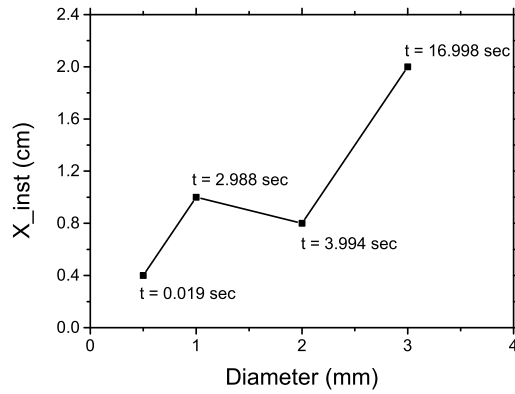
Figure 3.6: Location of first instability (X_{int}) formed with capillary diameter Ca_d, for its corresponding Re_c values. The time at which the initial instability was seen is shown in the graph.

at later times, for $1mm$ and $0.5mm$ diameter, the water occupied the whole domain and total displacement of coconut-oil by water was observed, Whereas the upper layer occupied by coconut-oil was thicker in $2mm$ and $3mm$ capillary diameter tubes. This type of phenomenon was also studied by many authors in core/annular flow in channels and capillaries, both numerically and experimentally. The axisymmetric behaviour of N-B type instability was seen for all the capillary diameter when the Re number was greater than 500, which is discussed in detail in the next section.

The location of first instability seen for a critical Reynolds number(minimum Re at which the instability is seen) in the capillary tube is shown in Fig 3.6. The graph was plotted for various diameters and their respective Re_c. From the Fig 3.6, it can be seen that for 0.5mm capillary diameter and corresponding $Re_c = 95$, the instability was seen to occur near the injection region $(0.4cm)$. Also the time taken for the first instability to occur for above given parameters was very less compared to the other capillary diameter. For $1mm$ and $2mm$ capillary diameter , the instability occurrence was seen to have increasing and decreasing behaviour respectively. For $3mm$ capillary diameter, the instability was seen to form far from the injection point$(2cm)$. As the capillary diameter goes on increasing, the time for first instability to occur was also seen to increase. Now we investigate the effect of Capillary diameter (Ca_d) on the flow dynamics discussed in the next section.

3.3.2   Effect of Ca_d

Now we investigate the effect of Capillary diameter (Ca_d) on the flow dynamics. In Fig 3.7, spatio-temporal evolution of the concentration field of water has been plotted at successive times (from top to bottom, $t = 10, 20, 30, 40$ and $t = 50$) for capillary diameter (a) 1mm, (b) 2mm and (c) 3mm. The rest of the parameter values are $Re = 120$ and length plotted for 1mm, 2mm and 3mm capillary diameter are (a) 8cm, (b) 10cm and (c) 15cm respectively. In Fig 3.7(c), compared to Fig 3.7(a)(b), it can be seen that the N-B type instability formation at t = 10 sec is just developing, whereas in 2mm and 1mm capillary diameter the N-B instability formation are 2 and 4 in count respectively. The N-B type instability formation, for constant Re, is seen to decrease as the capillary diameter is increased . Another interesting thing to notice is, the distance between two successive N-B type instability formation goes on increasing as the capillary diameter increases [30]. The reason behind it can be analysed as, the surface tension forces are less dominating as the capillary diameter increases. These surface tension forces are strong in small capillary diameters and tend to keep the water molecules in contact giving rise to more N-B type formation, whereas in large capillary diameters, the surface tension forces are less dominating and the finger elongates throughout the domain in cylindrical shape.

The instabilities formation is always seen to form near the lower wall of the capillary as shown in Fig 3.3 and Fig 3.7. As we decrease the capillary diameter and keeping other parameter constant, the axisymmetric nature of instability was seen more (Fig 3.7(a)(b)). This axisymmetric nature was also investigated in the present study for Fig 3.7, where image processing techniques (as described in section 3.2) were employed to calculate the values of R_u and R_l (Fig 3.2). From the values of R_u and R_l, the N-B instability thickness (NB_t) for different capillary diameter and time interval were obtained. The location of the instability for each capillary diameter was calculated by averaging the values of $(NB_t/2) + R_l$ for all the time interval. The averaged values of the instability location (from bottom wall) for 1mm, 2mm and 3mm capillary diameter was 0.47mm, 0.72mm and 1mm respectively. The values clearly depicts that as the capillary diameter is decreased, the instability
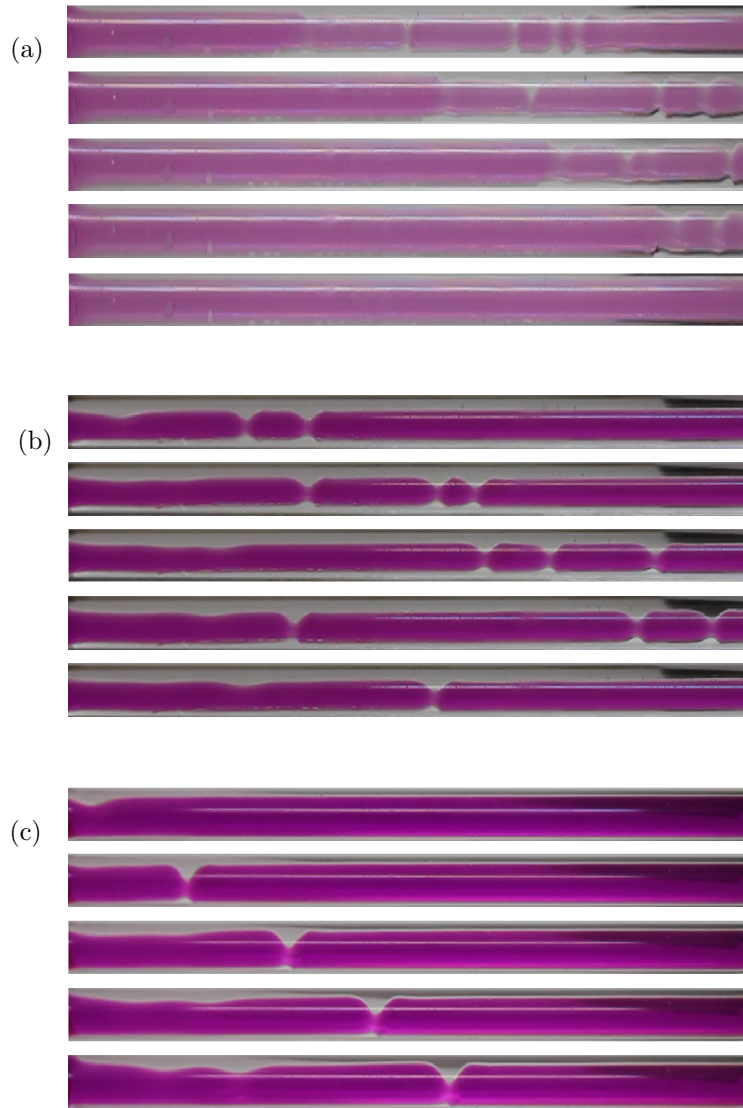
Figure 3.7: Experimental images of water penetrating inside the capillary at successive times (from top to bottom, $t = 10, 20, 30, 40$ and $t = 50$) for capillary diameter (a) 1mm, (b) 2mm and (c) 3mm. The rest of the parameter values are $Re = 120$ and length plotted for 1mm, 2mm and 3mm are (a) 8cm, (b) 10cm and (c) 15cm respectively (Water - pink colour and Coconut oil - transparent).

formation is seen near the mid-section of the radial direction, also giving rise to symmetric pattern.

In Fig 3.8, values of critical Reynolds number (Re_c) has been plotted for different capillary diameters(Ca_d). It is seen that as the diameter of the capillary decreases, the Re_c value also decreases. But when the capillary diameter reaches 0.5mm, the Re_c value increases and tends to deviate similar type of behaviour as other capillary diameters. The Re_c value for $Ca_d = 0.5$mm was found to be 95.

Figure 3.8: Variation of critical Reynolds number, Re_c, for $Ca_d = 3$mm, 2mm, 1mm and $D = 0.5$mm. The rest of the parameters are , $0 \leq t \leq 50$ sec and Aspect ratio $= 1 : 100$.

3.4   Concluding remarks

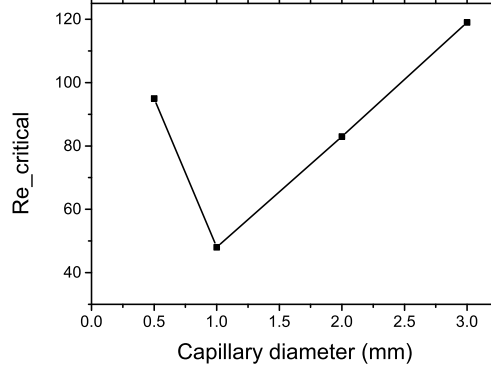The pressure-driven immiscible displacement flow, focusing on the situation where the invading fluid is less viscous than the resident fluid, is investigated experimentally in four different capillary tubes. The fluids considered here are water and coconut-oil with viscosity ratio, $\mu_{21} = 27$ and density ratio, $\rho_{21} = 0.925$. A parametric study has been conducted and influence of Reynolds number and Capillary diameter on the flow dynamics has been investigated. Our results demonstrate the presence of instability due to competition between imposed pressure gradient, gravity and surface tension forces. We found that, keeping other parameter constant and changing the capillary diameter, changes the critical Reynolds number (Re at which the first instability formation was observed). As the Reynolds number is decreased below the Re_c, plug flow displacement behaviour is observed in the system. In this, instability phenomenon is not continuous and formation of multiple plugs is observed. Initially the instability is "wavy" in structure and as the finger penetrates inside the capillary, a kink is observed. This kink type pattern is termed in this study as "Neck-break formation" (N-B). For $Ca_d \geq 1mm$, the gravity is the dominating force, which acts in the downward direction, settling the remnants of fluid "1" at the bottom part of the capillary tube, where as for $Ca_d < 1mm$, the effect of gravity is negligible. The time taken for first instability formation in the capillary tube is seen to increase with increase in Ca_d. For constant Re, the N-B type instability formation is decreased as the Ca_d is increased. As we decrease the capillary diameter, more axisymmetric nature of instability is observed . At micro scale, the flow dynamics observed in capillary tubes are very different than that as observed in macro scale. There is still a need to conduct research in this context and experiments need to be carried out to understand the "fluid flows in micro/nano scales".

References

[1] G. M. Homsy. Viscous Fingering in porous media, Annu. Rev 19, (1987) 271–311.

[2] R. L. Chuoke, P. van Meurs, and C. van der Poel. The instability of slow, immiscible, viscous liquid-liquid displacements in permeable media. *Petroleum Transactions, AIME* 216, (1959) 188–194.

[3] P. G. Saffman and G. Taylor. The Penetration of a Fluid into a Porous Medium or Hele-Shaw Cell Containing a More Viscous Liquid. *Proceedings of the Royal Society A: Mathematical, Physical and Engineering Sciences* 245, (1958) 312–329.

[4] C. T. Tan and G. M. Homsy. Stability of miscible displacements in porous media: rectilinear flow 29, 1986 3549–3556.

[5] K. C. Sahu and O. K. Matar. Stability of plane channel flow with viscous heating. *Journal of Fluids Engineering* 132, (2010) 11202.

[6] R. Govindarajan and K. C. Sahu. Instabilities in Viscosity-Stratified Flow. *Annual Review of Fluid Mechanics* 46, (2014) 331–353.

[7] M. Mishra, P. M. J. Trevelyan, C. Almarcha, and A. De Wit. Influence of double diffusive effects on miscible viscous fingering. *Physical Review Letters* 105, (2010) 204501.

[8] K. C. Sahu. Double diffusive effects on pressure-driven miscible channel flow: Influence of variable diffusivity. *International Journal of Multiphase Flow* 55, (2013) 24–31.

[9] M. Mishra, A. De Wit, and K. C. Sahu. Double diffusive effects on pressure-driven miscible displacement flows in a channel. *Journal of Fluid Mechanics* 712, (2012) 579–597.

[10] K. C. Sahu and R. Govindarajan. Spatio-temporal linear stability of double-diffusive two-fluid channel flow. *Physics of Fluids* 24, (2012) 529–539.

[11] K. C. Sahu. A review on double-diffusive instability in viscosity stratified flows. *Proc. Indian Nat. Sci. Acad* 80, (2014) 513–514.

[12] S. Ghosh, R. Usha, and K. C. Sahu. Double-diffusive two-fluid flow in a slippery channel: A linear stability analysis. *Physics of Fluids* 26, (2014) 015412.

[13] S. Ghosh, R. Usha, and K. C. Sahu. Linear stability analysis of miscible two-fluid flow in a channel with velocity slip at the walls. *Physics of Fluids* 26, (2014) 014107.

[14] J. S. Turner. Double-Diffusive Phenomena. *Annual Review of Fluid Mechanics* 6, (1974) 37–54.

[15] K. C. Sahu and R. Govindarajan. Stability of flow through a slowly diverging pipe. *Journal of Fluid Mechanics* 531, (2004) 325–534.

[16] T. Radko and M. E. Stern. Finescale Instabilities of the Double-Diffusive Shear Flow*. *Journal of Physical Oceanography* 41, (2011) 571–585.

[17] B. T. Ranganathan and R. Govindarajan. Stabilization and destabilization of channel flow by location of viscosity-stratified fluid layer. *Physics of Fluids* 13, (2001) 1–3.

[18] P. Ern, F. Charru, and P. Luchini. Stability analysis of a shear flow with strongly stratified viscosity. *Journal of Fluid Mechanics* 496, (2003) 295–312.

[19] E. J. Hinch A note on the mechanism of the instability at the interface between two shearing fluids, J. Fluid Mech.. *Journal of Fluid Mechanics* 144, (1994) 463–465.

[20] M. J. South and a. P. Hooper. Linear growth in two-fluid plane Poiseuille flow. *Journal of Fluid Mechanics* 381, (1999) 121–139.

[21] S. V. Malik and A. P. Hooper. Linear stability and energy growth of viscosity stratified flows. *Physics of Fluids* 17, (2005) 1–8.

[22] B. Selvam, S. Merk, R. Govindarajan, and E. Meiburg. Stability of miscible coreannular flows with viscosity stratification. *Journal of Fluid Mechanics* 592, (2007) 23–49.

[23] B. Selvam, L. Talon, L. Lesshafft, and E. Meiburg. Convective/absolute instability in miscible core-annular flow. Part 2. Numerical simulations and nonlinear global modes. *Journal of Fluid Mechanics* 618, (2009) 323–348.

[24] K. C. Sahu, H. Ding, P. Valluri and O. K. Matar. Linear stability analysis and numerical simulation of miscible two-layer channel flow. *Physics of Fluids* 21, (2009) 042104.

[25] K. C. Sahu, H. Ding, and O. K. Matar. Numerical simulation of non-isothermal pressure-driven miscible channel flow with viscous heating. *Chemical Engineering Science* 65, (2010) 3260–3267.

[26] D. D. Joseph, R. Bai, K.P Chen and Y.Y Renrdy. Core-Annular Flows. *Annual Review of Fluid Mechanics* 29, (1997) 65–90.

[27] B. Jha, L. Cueto-Felgueroso, and R. Juanes. Quantifying mixing in viscously unstable porous media flows. *Physical Review E - Statistical, Nonlinear, and Soft Matter Physics* 84, (2011) 066312.

[28] B. Jha, L. Cueto-Felgueroso, and R. Juanes. Fluid mixing from viscous fingering. *Physical Review Letters* 106, (2011) 194502.

[29] W. Kuhn. {Ü}ber die Gestalt fadenf{ö}rmiger Molek{ü}le in L{ö}sungen. *Kolloid-Zeitschrift* 68, (1934) 2–15.

[30] W. K. Chan and C. Yang. Surface-tension-driven liquidliquid displacement in a capillary. *Journal of Micromechanics and Microengineering* 15, (2005) 1722.

[31] S. Popinet. Gerris: a tree-based adaptive solver for the incompressible Euler equations in complex geometries. *J. Comput. Phys* 190, (2003) 572–600.

[32] M. K. Tripathi, K. C. Sahu, and R. Govindarajan. Why a falling drop does not in general behave like a rising bubble. *Scientific reports* 4, (2014) 4771.

[33] M. K. Tripathi, K. C. Sahu, G. Karapetsas, K. Sefiane, and O. K. Matar. Non-isothermal bubble rise: non-monotonic dependence of surface tension on temperature. *Journal of Fluid Mechanics* 763, (2015) 82–108.

[34] M. K. Tripathi, K. C. Sahu, and R. Govindarajan. Dynamics of an initially spherical bubble rising in quiescent liquid. *Nature Communications* 6, (2015) 6268.

[35] G. I. Taylor. Deposition of viscous fluid on the wall of a tube. *Journal of Fluid Mechanics* 10, (1961) 1961.

[36] C.S. Yih. Instability due to viscosity stratification. *Journal of Fluid Mechanics* 27, (1967) 337.

[37] P. R. Redapangu, K. Chandra Sahu, and S. P. Vanka. A Lattice Boltzmann Simulation of Three-Dimensional Displacement Flow of Two Immiscible Liquids in a Square Duct. *Journal of Fluids Engineering* 135, (2013) 121,202.

[38] J. Chin, E. S. Boek, and P. V. Coveney. Lattice Boltzmann simulation of the flow of binary immiscible fluids with different viscosities using the Shan-Chen microscopic interaction model. *Philosophical Transactions of the Royal Society of London A* 360, (2002) 547–558.

[39] P. Grosfils, J. P. Boon, J. Chin, and E. S. Boek. Structural and dynamical characterization of Hele-Shaw viscous fingering. *Philosophical transactions. Series A, Mathematical, physical, and engineering sciences* 362, (2004) 1723–34.

[40] Q. Kang, D. Zhang, and S. Chen. Immiscible displacement in a channel: Simulations of fingering in two dimensions. *Advances in Water Resources* 27, (2004) 13–22.

[41] B. Dong, Y. Y. Yan, W. Li, and Y. Song. Lattice Boltzmann simulation of viscous fingering phenomenon of immiscible fluids displacement in a channel. *Computers and Fluids* 39, (2010) 768–779.

[42] B. Kettlitz. M. J. Lewis: Physical Properties of Foods and Food Processing Systems. *Food / Nahrung* 33, (1989) 103–103.

[43] J. P. Stokes, D. A. Weitz, J. P. Gollub, A. Dougherty, M. O. Robbins, P. M. Chaikin, and H. M. Lindsay. Interfacial Stability of Immiscible Displacement in a Porous Medium. *Phys. Rev. Lett.* 57, (1986) 1718–1721.

[44] S. J. Smith and C. T. Friedrichs. Image processing methods for in situ estimation of cohesive sediment floc size, settling velocity, and density. *Limnology and Oceanography: Methods* 250–264.

[45] M. E. Charles and L. U. Lilleleht. An experimental investigation of stability and interfacial waves in co-current flow of two liquids. *Journal of Fluid Mechanics* 22, (1965) 217–224.

[46] M. Cloupeau and B. Prunet-Foch. Electrostatic spraying of liquids: Main functioning modes. *Journal of Electrostatics* 25, (1990) 165 – 184.

[47] P. R. Redapangu, K. Chandra Sahu, and S. P. Vanka. A study of pressure-driven displacement flow of two immiscible liquids using a multiphase lattice Boltzmann approach. *Physics of Fluids* 24, (2012) 10.